Complex Fluid-Fluid Interfaces: Rheology and Structure

Gerald G. Fuller[1] and Jan Vermant[2]

[1]Department of Chemical Engineering, Stanford University, Stanford, California 94305-5025; email: ggf@stanford.edu

[2]Department of Chemical Engineering, University of Leuven, Leuven B-3001, Belgium; email: Jan.Vermant@cit.kuleuven.be

Annu. Rev. Chem. Biomol. Eng. 2012. 3:519–43

First published online as a Review in Advance on April 23, 2012

The *Annual Review of Chemical and Biomolecular Engineering* is online at chembioeng.annualreviews.org

This article's doi: 10.1146/annurev-chembioeng-061010-114202

1947-5438/12/0715-0519$20.00

Keywords

stability, foams, emulsions, surface tension

Abstract

Complex fluid-fluid interfaces are common to living systems, foods, personal products, and the environment. They occur wherever surface-active molecules and particles collect at fluid interfaces and render them nonlinear in their response to flow and deformation. When this occurs, the interfaces acquire a complex microstructure that must be interrogated. Interfacial rheological material properties must be measured to appreciate their role in such varied processes as lung function, cell division, and foam and emulsion stability. This review presents the methods that have been devised to determine the microstructure of complex fluid-fluid interfaces. Complex interfacial microstructure leads to rheological complexity. This behavior is often responsible for stabilizing interfacial systems such as foams and emulsions, and it can also have a profound influence on wetting/dewetting dynamics. Interfacial rheological characterization relies on the development of tools with the sensitivity to respond to small surface stresses in a way that isolates them from bulk stresses. This development is relatively recent, and reviews of methods for both shear and dilatational measurements are offered here.

1. INTRODUCTION

Interfaces between two fluids occur just about everywhere, be it in nature or in industrial applications. They are used to provide structure to chemical products and occur in several basic processes in the chemical industry, such as liquid-liquid extraction or flotation. When the fluids are pure and simple, a single value of the surface tension suffices to characterize the interface (1). However, in most technological or biological applications, amphiphilic molecules such as surfactants, proteins, particles, or macromolecules will populate the interfaces. For such complex fluid interfaces, a single value of the interfacial tension is no longer a sufficient descriptor. Apart from possible thermodynamic complexities associated with interfaces, chemical and biological engineers know well that we need to look at interfacial transport phenomena both across and within the complex interface (2). In his classical treatment on thermodynamics of heterogeneous systems, J.W. Gibbs distinguished between a surface tension and a surface stress (3). Indeed, restricting particles, macromolecules, or surfactants to an interface induces microstructures with significant mechanical strength. These structures can strongly couple to hydrodynamic forces, resulting in nonlinear rheological properties and complex constitutive relations linking the deformations of the interface to the surface stress. In such cases we need to go beyond the Young-Laplace equation to describe the response of the fluid-fluid interface.

Classically, applications of complex fluid interfaces in emulsions and foams have been a focus. A substantial literature deals with the effects of surfactants on emulsion and foam stability. They are well known for lowering surface tension, but the dynamics of adsorption and desorption of the surfactants also play an important role in the increased resistance of the interface to deformation (4). More recently, attention has shifted to the role of the interfacial rheological properties, and the elasticity of surfactant and protein-laden interfaces in particular, in determining the stability of emulsions and foams (5–7). This research has of course been driven by applications in consumer care products but also by structural design in foods (8) and enhanced oil recovery (9). In the past ten years increased interest has been directed toward the use of solid particles as alternatives to surfactants to produce solid-stabilized Pickering-Ramsden emulsions (10, 11) or solid-stabilized foams (10, 12). The effect of particles on the interfacial tension is far less pronounced compared with that of surfactants, but they can significantly contribute to the development of an interfacial stress, as these 2D suspensions have rheological properties similar to those of their 3D counterparts (13, 14). Even more intricate aspects of dynamics come into play as two particle-laden interfaces interact (15). An area of development is the use of particles to stabilize other types of thin-film flows; an intriguing example is how the use of ellipsoidal particles that assemble and rigidify the interface can prevent the coffee ring stain effect (16). Other areas of interesting development include the use of interfacially trapped particles in bicontinuous particle gels (17) and in functional polymer-polymer nanocomposites (18). One of the most striking examples of how particles modify interfacial dynamics is the so-called liquid marbles in which the fluid encapsulated by particles is a liquid and the fluid in which it is immersed is air (19, 20). These liquid marbles have potential applications for the encapsulation of low–surface tension liquids and their subsequent use as miniature reactors (21). Furthermore, one can invert the situation to create a foam consisting of particle-stabilized gas pockets within water, sometimes referred to as dry water droplets (22), which have potential application in either the storage or controlled release of gases (20).

In the past ten years chemical engineering as a field has embraced the study of complex fluid interfaces in the biological sciences, where a vast range of problems relate to the link between dynamics and structure. The most prominent example is the membranes of living cells. These are formed from phospholipid bilayers (23) and, similar to other vesicles, define an interface between two regions of essentially the same fluid, as opposed to emulsions that are comprised of immiscible

fluids. However, these membranes effectively control the transport of solutes across the interface. Processes such as cell division and the transport of blood cells through small capillaries (24) depend on the rheological properties of the membrane. The alveoli within the lung (25) and the meibomian lipid layer on the tear film (26) are other examples in which the response to dynamic deformation of biological films plays a key role in the proper function of living systems. Also, bacteria and fungi secrete molecules that are surface active and form a complex fluid interface atop a biofilm or bacterial swarm. Gradients in the concentration of surface-active materials drive a convective motion (27, 28). Recent experiments have shown nicely how bacteria "surf the waves" induced by gradients in surface tension (29). This review aims to identify several common features of chemical and biological problems related to complex fluid interfaces.

2. BRIEF HISTORICAL OVERVIEW

One of the first accounts of complex fluid-fluid interfaces dealt with the "stilling of the waves" by oil as described by Pliny the Elder (77 AD) and later investigated in detail by Benjamin Franklin (30, 31), Lord Rayleigh (32), and Agnes Pockels (33). Another important contribution came from Joseph Plateau (34) in a series of papers published in 1873. He was the first to prove experimentally that molecular forces act in a thin surface layer and to claim the existence of a surface viscosity. He compared the damping of a magnetic compass needle on a bare and a on a surfactant-laden interface (34). However, as Marangoni (35) pointed out, the rotating needle sweeps the interface, thereby creating a concentration gradient. Marangoni proposed a modified device with a solid brass disc and was not able to measure any significant surface viscosity difference between a bare and a surfactant-laden interface. To resolve the issue, Lord Rayleigh (36) designed an experiment with a ring, which taught us the importance of reducing the area of the measurement geometry in contact with the subphase and avoiding concentration gradients.

Boussinesq (37) introduced interfacial, rheological material functions to explain observations that small drops and bubbles often translate through a liquid under the action of gravity with the same speed as though they were solid spheres, as identified in experiments by Lebedev (38) and Silvey (39). However, a chemical engineer, L.E. "Skip" Scriven (40), properly set down the equations describing the conservation of momentum at fluid/fluid interfaces in 1960. Scriven also established the constitutive equation for a Newtonian interface—a relationship now referred to as the Boussinesq-Scriven constitutive equation.

3. THERMODYNAMICS AND CAPILLARITY

The interfaces between a liquid and its surroundings are characterized by surface energies, σ, first introduced by Gibbs (3). One particular result that reveals an important aspect of complex fluid-fluid interfaces is the calculation of the increment in pressure, Δp, caused by a tangential surface stress, τ, acting on a curved, liquid surface. A simple force balance immediately leads to

$$\Delta p = \tau \left(\frac{1}{R_1} + \frac{1}{R_2} \right), \qquad 1.$$

where R_1 and R_2 are the local radii of curvature and τ is the surface stress acting at that point. Gibbs first proposed the surface stress function, τ, but often it is substituted by surface energy, σ. With that replacement, Equation 1 is called the Young-Laplace equation. However, this substitution is strictly allowable only for a pure, liquid interface. Shuttleworth (41) considered the case in which an interface can respond to a surface strain, ε, with a corresponding surface stress; he produced

the following relationship between these two functions:

$$\tau = \sigma + \frac{\partial \sigma}{\partial \varepsilon}, \qquad 2.$$

or, in the more general case in which the stress and strain are more properly represented as tensors,

$$\tau_{ij} = \sigma \delta_{ij} + \frac{\partial \sigma}{\partial \varepsilon_{ij}}. \qquad 3.$$

Another term that is used is surface tension, which has the same units as surface energy. In the restricted case of a one-component, pure liquid, Rayleigh (42) demonstrated that these two quantities are equivalent. However, the more general description employing the surface stress tensor is preferred when describing complex fluid-fluid interfaces that can support anisotropic stresses.

When this equation is applied to a pendant droplet, it can be used to determine the surface energy, but this is strictly possible only when the surface stress tensor and the surface energy are equivalent. This restriction becomes particularly important when the pendant drop configuration is used to determine interfacial dilatational rheological properties. This point will be taken up further in Section 6.

Broadly, fluid interfaces in the presence of amphiphiles are divided into two classes: soluble materials that produce Gibbs monolayers and insoluble, surface-active materials that form Langmuir films. When monolayers arise from soluble materials, the surface concentration of a species, Γ_i, is related directly to its bulk concentration, c_i, and at equilibrium and low concentration, Gibbs arrived at the following formula:

$$\Gamma_i = -\frac{1}{RT}\left(\frac{\partial \sigma}{\partial \ln c_i}\right)_{T,P}. \qquad 4.$$

Insoluble monolayers frequently occur. Examples include 2D gels formed by associating proteins (43), amphiphilic polymer chains (44), phospholipids (23), fatty alcohols (45), and fatty acids (46). The constraint of confinement to an interface forces lateral order in the layer, which results in rich phase behavior. The thermodynamic behavior of these materials is normally explored using a Langmuir trough, a classic apparatus in surface science that allows systematic variation of the available area, A, and the surface pressure, calculated as $\Pi = \sigma_0 - \sigma$, where σ_0 is the surface tension of the clean, bare interface in the absence of a film. Typically, the surface pressure is determined as a function of area at a specified temperature to obtain a $\Pi - A$ isotherm. Overall, the surface pressure is increased as the layers are compressed. However, phase transitions can appear as discontinuities in slope, and even plateaus in the case of first-order transitions.

An isotherm illustrating such a transition for two isomeric forms of 4-octyl-4′,8-(3-carboxytrimethyleneoxy) azobenzene (C_8AzC_3) is shown in **Figure 1** (47). This is a fatty acid containing azobenzene that causes a *trans*-to-*cis* conformational change upon irradiation with UV-visible light. Curve *a* in the figure was taken on a monolayer containing this molecule in the *trans* configuration after illumination with visible light. In this state, the molecules can pack efficiently, and a first-order phase transition is evident at a surface pressure of approximately 14 mN m^{-1}. Applying UV radiation converts the molecule to its *cis* form, which has an expanded area per molecule and is unable to pack densely. The isotherm for this state lacks a first-order transition and reflects a much more compressible monolayer.

The inset plot in **Figure 1** shows the isotherm for a C22 fatty acid, docosanoic acid (DA), also known as behenic acid. This well-studied molecule also exhibits a first-order transition at approximately $\Pi = 15$ mN m^{-1} and another transition at approximately $\Pi = 25$ mN m^{-1}. Detailed structural measurements on this molecule using grazing incidence x-ray diffraction

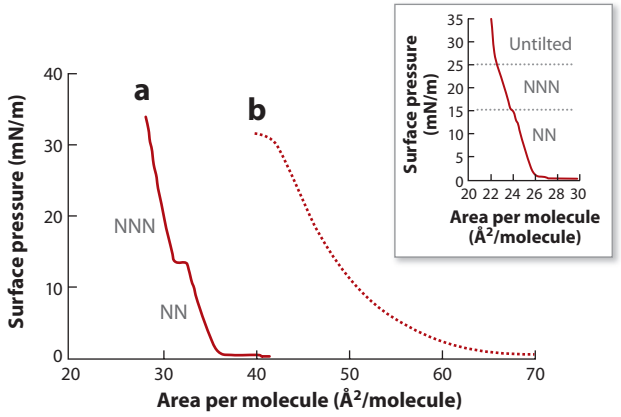

Figure 1

Surface pressure-area isotherms for 4-octyl-4′,8-(3-carboxytrimethyleneoxy) azobenzene (C_8AzC_3) monolayers at 22°C. (*a*) *Trans* isomer. (*b*) *Cis* isomer after 10 min of 365-nm irradiation (1 mW cm^{-2}). (*Inset*) An isotherm of docosanoic acid at 15°C. Abbreviations: NN, nearest neighbor; NNN, next nearest neighbor. From Kim & Fuller (47), *Phys. Rev. E*, 67:041061. Copyright © 2003 by the American Physical Society.

(GIXD) (48), which is described in Section 4, reveal that this molecule self-assembles by placing its head groups on a distorted hexagonal lattice. Furthermore, these transitions register conversions in the tilt azimuth of this molecule. The lower-pressure transition is from a nearest-neighbor (NN) tilt toward a next-nearest-neighbor tilt (NNN). At the higher-pressure transition, the tilt angle is eliminated, and the molecules extend straight upward. The nomenclature for the phases of these structured films follows the liquid crystal literature; the lower-pressure phase is called the L_2 phase. The NNN phase is called the L_2' phase. In the absence of detailed structural data, phases encountered in Langmuir isotherms are often simply referred to as the "liquid expanded phase" at lower surface pressures following a first lift-off from zero surface pressure and as the "liquid condensed phase" following the first indication of a phase transition. As described in Section 7.1, each of these phases can have a distinct response to interfacial stresses and flow.

Capillary forces are central to many observed phenomena and drive numerous interfacial flow phenomena; these are discussed in Section 5. They also are of prime importance in layers of particles attached to liquid surfaces. First, they can effectively pin particles to the interface and make their expulsion difficult. The energy to remove a sphere from an oil/water interface that is attached by a contact angle, θ (measured from the water side), is (49) $\Delta E = \pi r^2 \sigma_{ow}(1 \mp \cos\theta)^2$, where the negative sign is used when the particle is removed into the water and the plus sign indicates particle removal into the oil. The interfacial tension, σ_{ow}, is between the oil and the water, and r is the sphere radius. For micrometer-sized particles, these energies are large—on the order of millions of kT.

When two particles are located at a liquid interface, deflections of the interface by the presence of the particles interact and generate a net attractive force that causes the particles to move together. Kralchevsky and coworkers (50) have analyzed this problem for particles that deform the interface by buoyancy forces. As the particles approach one another, the deformation of the interface between the particles is diminished, and the interfacial tension force vectors between the particles become more parallel to the surface. Kralchevsky and coworkers (50) showed that in the limit of a large interparticle separation distance, L, the force acting on a pair of particles is $F \approx 1/L$. This approximate result has been verified experimentally for non-Brownian particles with a density difference with the suspending liquid.

The morphology of multiphasic monolayer systems is also affected by line tension, $\Im$, which plays an analogous role to surface tension in 2D systems. Line tension, which has the dimensions of energy per unit length, acts along the perimeter between phases within a surface. In other words, a curved line with radius of curvature r defining the boundary between separate phases within a surface can be expected to give rise to a differential surface pressure on the order of $\Delta\Pi \approx \Im/r$. In most cases, the magnitude of the line tension is expected to be on the order of $\Im \approx \sigma a$, where a is on the order of the molecular size (a few angstroms) (51). Although this effect is not significant for colloidal particles residing at interfaces, it plays an important role in determining the shape of domains in molecular monolayers of phospholipids as well as in fatty acids and alcohols. McConnell (23) has studied its role in this regard extensively, and more recently Stone & McConnell (52) analyzed it quantitatively by modeling time-dependent transitions in domain shape by taking into account the opposing forces of dipole-dipole repulsions within domains and the restoring influence of line tension.

4. MEASUREMENT OF INTERFACIAL MICROSTRUCTURE

Section 7 presents the interfacial rheological responses of a variety of complex fluid-fluid interfaces, revealing that strong, nonlinear behavior is observed. It is important to appreciate the microstructural origins causing these mobile layers to couple so strongly to interfacial stresses and strains, and several experimental tools can be brought to bear on this problem. The methods reviewed are optical, and many take advantage of successful techniques developed for bulk materials. Others are designed strictly to probe interfacial systems.

Simple optical microscopy is particularly useful for particle-laden interfaces, which are discussed in Section 7.3. The choice of whether to use an upright or an inverted microscope depends on several factors, including the spatial constraints imposed by the types of flow cells used to generate the interfacial flows. Three types of flow geometries have been used in the majority of past work: interfacial flow-through devices to generate channel flows and flows through complex geometries (53, 54), the parallel band apparatus to simulate simple shear flow (55, 56), and the four-roll mill (57, 58). Images taken using bright field microscopy can be exploited to extract details of local structure in 2D suspensions. In layers of aggregating particles, the distribution of aggregate size can be acquired along with coordination numbers (59, 60). As discussed in Section 7.3, many particle systems trapped at interfaces resist aggregation, and the radial distribution function of stable 2D dispersions can be determined using data from optical microscopy images (61).

The power of optical microscopy can be enhanced through the addition of fluorescence optics, which allows one to track the fate of components in mixtures with the use of fluorescent dyes. These dyes can be forced to associate with specific components in a mixture through chemical labeling or by a natural affinity toward different constituents or phases. In an example of chemical attachment, the Dai group (62) followed arrays of polystyrene spheres attached to oil droplets (polydimethylsiloxane) residing in water using fluorescence imaging. In addition, Clegg and coworkers (63) recently used this method to reveal the bicontinuous microstructure of a binary liquid undergoing spinodal decomposition in the presence of particles that are attracted to the interface of these biphasic systems. Epifluorescence microscopy has long been used to reveal the microstructure of biphasic phospholipid monolayers by adding a trace amount of amphiphilic dye molecules that are preferentially displaced from a liquid condensed phase in favor of residing within a coexisting liquid expanded phase. An epifluorescence microscope can then be used to display the domain structure of such a biphasic monolayer (23). **Figure 2** presents images for a 1,2-dipalmitoyl-*sn*-glycero-3-phosphocholine (DPPC) monolayer in the liquid expanded phase.

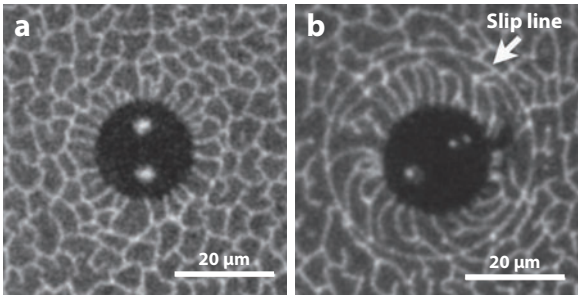

Figure 2

Fluorescence microscopy of 1,2-dipalmitoyl-*sn*-glycero-3-phosphocholine (DPPC) monolayers showing (*a*) interlocked liquid condensed domains prior to deformation and (*b*) the creation of a slip line upon rotation of the disc. Figure adapted from Choi et al. (64).

However, the system is polydomain, and the dye molecules accumulate at the grain boundaries separating the domains (64). The circular object at the center is a magnetic button, which can be forced to rotate in response to a rotating magnetic field. **Figure 2*a*** shows the domain structure undeformed for an applied torque below that necessary to overcome a yield stress. However, above this stress, the button is able to rotate, as is indicated by the white arrow in **Figure 2*b***. Indeed, the deformation of the domain structure is nonuniform and reveals a slip line at a certain radial distance from the button, as indicated by the white arrow. Within this region, the button and attached domains rotate as a rigid body. However, beyond the slip line, no motion is produced (64).

Brewster angle microscopy (BAM) is an imaging method that is particularly well-suited to fluid interfaces and was simultaneously presented by Meunier & Hénon (65) and Hönig & Möbius (66) in 1991. It relies on the existence of a Brewster angle, ϕ_B, for the clean interface of interest at which light polarized in the plane of incident (*p*, polarized light) is not reflected. However, once the same interface supports a film, the Brewster angle condition will be violated, and light will be reflected. Capture of this reflected light onto an area detector provides an image of the film. The first application of BAM to analyze Langmuir films subject to flow considered the response of DA to elongational flow generated using a four-roll mill (57); BAM revealed flow-induced reorientation of the tilt azimuth of the tilted aliphatic tails of this molecule in the L_2' phase.

The imaging methods described above are appropriate for microscopic length scales on the order of micrometers. For measurement of molecular-level organization and orientation, GIXD and dichroism have been used. Dichroism refers to polarization-dependent anisotropy in the optical absorption of a material and has been employed extensively in the study of bulk materials; Fuller (67) describes its application to flow-induced orientation in complex fluids. Polarization modulation dichroism methods offer enhanced sensitivity (67), and the proper choice of wavelength has made flow-induced molecular orientation of monolayers possible for several materials. For example, the rigid macromolecule poly(*p*-phenylene) sulfonic acid (PPPSH) absorbs strongly in the UV, and Fuller and coworkers used the 275-nm line of an argon-ion laser to examine isotropic-to-nematic transitions of PPPSH monolayers (68). When the amphiphiles of interest do not offer an intrinsic, strong absorption, dye molecules often can be attached to provide the required anisotropic absorbance. For example, Goffin et al. (69) incorporated the dye sirius red F3B in studies of flow orientation of multilayers of collagen fibers.

The constituent molecules of insoluble monolayers of fatty acids, fatty alcohols, and phospholipids often self-assemble to form a variety of ordered morphologies, and grazing incidence x-ray reflection (GIXR) and GIXD have been utilized to extract the details of that molecular

organization. Accounts of the use of these powerful tools can be found in several reviews (48, 70–72). X rays interact with the electron distribution of the sample. GIXR measurements capture the intensity of x rays that are specularly reflected from the interface and are directly related to the Fourier transform of the gradient of the electron density profile along the depth direction, z. Once the reflected light intensity is measured as a function of the vector component, q_z, these data can be fit to models of the electron distribution. From such fittings, the mean layer thickness and tilt angle of the molecules can be determined.

GIXD measurements capture the intensity of x rays that are diffracted from periodic structures in the plane of the surface using a position-sensitive detector. These periodic structures arise from the positional order of the head groups as they assemble into lattices. Bragg rods that are oriented along the z (vertical) axis and positioned at the reciprocal space lattice locations of the film produce the diffracted light. Als-Nielsen & Kjaer (48) discuss the analysis of the diffraction patterns in detail and explain how these data can be used to determine the lattice geometry of the head groups and the tilt azimuth of the aliphatic tails of amphiphiles.

5. INTERFACIAL FLUID DYNAMICS

The study of interfacial rheology requires consideration of flows occurring at liquid interfaces. In addition, surface stresses occurring at these interfaces can induce a variety of flow phenomena and fluid instabilities. For fluid interfaces that are characterized solely by surface tension, the basis for these flows is captured by the following classic boundary condition that must be satisfied at the interface separating two fluids:

$$\left(\tau_{ij}^{(1)} - \tau_{ij}^{(2)}\right) n_j + \frac{\partial \sigma}{\partial x_i} - \sigma(\nabla \cdot \mathbf{n}) n_i = 0, \qquad 5.$$

where the superscripts 1 and 2 refer to the separate fluid phases on either side of the interface. This condition requires that two surface tension contributions balance the stress differences across the interface. The second term in Equation 5 arises from spatial gradients in surface tension that cause shear stresses in the surrounding bulk fluids. These result in Marangoni flows that are responsible for a variety of commonly observed phenomena, such as the tears appearing in glasses of wine (73–75). The last term in Equation 5 predicts that normal stress differences will result when surface tension acts on a curved surface. Indeed, because $(\nabla \cdot \mathbf{n})$ calculates twice the mean curvature of a surface, this term is equivalent to the Young-Laplace pressure.

Numerous examples also exist of flow phenomena linked to the appearance of normal stresses when surface tension exerts itself across curved interfaces. These stresses are responsible for the capillary thinning of liquid filaments (76, 77). In this process, capillary forces pump liquid away from the necks of liquid filaments, which causes them to constrict to the point of breakage, and subjects the liquid to extensional deformations. For this reason, this flow phenomenon has been used to evaluate the elongational viscosities of complex liquids. Related to capillary thinning is the Plateau-Rayleigh instability of liquid cylinders, whereby such cylinders spontaneously break up into sequences of equally sized droplets (78), and the Rayleigh-Taylor instability of thin liquid films (79).

The flows that result from either Marangoni stresses or Young-Laplace pressures can be present in some measurements of interfacial rheology, and care must be taken to properly account for their possible influence. For example, in surface dilatational measurements, the expansion of fluid interfaces will create new surface area, and gradients in surface concentration can ensue. If this occurs, the resulting Marangoni stress can adversely affect the determination of dilatational rheology.

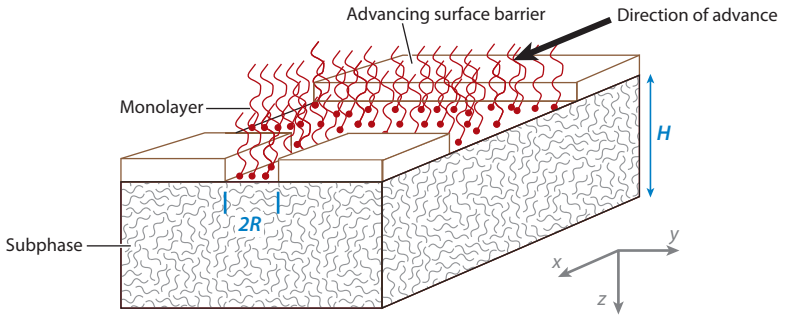

Figure 3

The channel flow of a monolayer pushed through a parallel constriction with a gap width of $2R$ by a surface barrier. The depth of the subphase (normally water) is H.

However, interfacial shear rheometry is normally conducted at constant surface area, and surface concentration gradients often can be neglected. In these measurements, interfacial flows are generated either by moving solid boundaries within the interface or by applying gradients in surface pressure. Analysis of the resulting flows requires accounting for the coupling of the surface and bulk fluid stresses. Schwartz et al. (53) accomplished this for the problem described in **Figure 3**. They carried out this analysis in the limit of small Boussinesq numbers ($Bo \ll 1$) for a purely viscous monolayer. This dimensionless group, which is the ratio of interfacial stresses to bulk stresses, is central to interfacial rheology and has the form

$$Bo = \frac{\eta_s}{\eta L}, \qquad 6.$$

where η_s is the interfacial shear viscosity, η is the shear viscosity of the bulk, and L is a length scale appropriate to the geometry of a given problem. Formally, this length scale is the ratio of the area over which bulk stresses are applied to the perimeter acted on by surface stresses.

The surface flow is generated by advancing the surface barrier toward a channel formed by parallel, stationary barriers that are separated by a gap of width $2R$. This sets up a surface pressure gradient, $\partial\Pi/\partial y$, along the channel that drives a surface flow. The length of the channel is taken to be sufficiently large relative to the gap so that a fully developed surface flow is established. Two velocity fields require solution, the velocity field in the subphase, $\mathbf{u} = (u, 0, 0)$, and the monolayer velocity field, $\mathbf{u}_s = (u_s, 0, 0)$. The bulk-phase velocity field satisfies the Stokes equation, and in the absence of a pressure gradient applied to the bulk, this reduces to $d^2u/dy^2 = 0$. This must satisfy a no-slip boundary condition at the bottom of the container, $u(x, y, z = H) = 0$, and a matching of stresses at the monolayer surface. The governing equation for the monolayer is

$$\eta_s \frac{d^2u_s}{dy^2} - \frac{d\Pi}{dx} + \eta \left(\frac{\partial u}{\partial z}\right)_{z=0} = 0; \quad |y| < R, \qquad 7.$$

where the third term couples the monolayer to the bulk phase.

In the limit of small values of the Boussinesq number, the flow at the interface is

$$u_s = -\frac{R}{\eta}\left(\frac{\partial\Pi}{\partial x}\right)\sqrt{1 - \frac{y^2}{R^2}}. \qquad 8.$$

Schwartz et al. (53) accompanied this analysis with experimental observations. The surface viscosities of the specific systems used put their experiments in the low Boussinesq limit, and excellent agreement with Equation 8 was found.

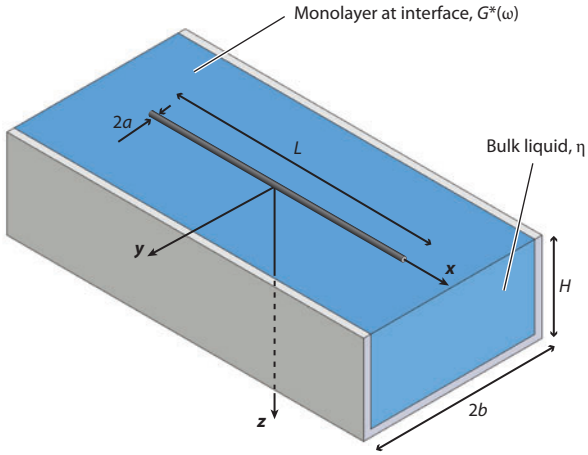

Figure 4

A cylindrical rod of length L and diameter a floating at the interface of a liquid with a complex surface modulus $G^*(\omega)$ that fills a rectangular container of width $2b$ and depth H. Oscillation of the rod along its axis at a frequency ω induces a shearing flow at the interface.

Soon after, Stone (80) considered the monolayer channel flow problem but without the limitation of a small Boussinesq number. That analysis predicted that the monolayer velocity profile evolves from the low Boussinesq limit given by Equation 8 to the following form at high values of this dimensionless group ($Bo \gg 1$):

$$u_s = -\frac{R^2}{\eta_s}\left(\frac{\partial \Pi}{\partial x}\right)\left(1 - \frac{y^2}{R^2}\right). \qquad 9.$$

However, these results are applicable only for purely Newtonian interfaces characterized by a constant surface viscosity, η_s, and no elasticity. When Kumaz & Schwartz (81) applied the same flow field to a monolayer of arachidic (eicosanoic) acid, which has a liquid crystalline character (57), unique, triangular-shaped velocity profiles were found in the channel flows.

Another important interfacial flow is associated with the interfacial stress rheometer (ISR) based on a rod forced to glide along an interface when contained within a channel (**Figure 4**). Vermant and colleagues (82) solved this problem recently by approximating the rod as a line source of force within the monolayer. Because it is of interest to solve for oscillatory, time-dependent flows for this rheometer, the governing equation for the bulk phase becomes

$$\rho\frac{\partial u}{\partial t} = \eta\frac{\partial^2 u}{\partial y^2}, \qquad 10.$$

but this is subject to no-slip boundary conditions on all solid boundaries of the submerged channel. The presence of the oscillating rod changes the governing equation for the monolayer to

$$\eta_s\frac{\partial^2 u_s}{\partial y^2} + \eta\left(\frac{\partial u}{\partial z}\right)_{z=0} + f(t)\delta(y) = 0, \qquad 11.$$

where $f(t)$ is the time-dependent force per unit length on the rod and is taken to be $f(t) = f_0 \cos \omega t$ (82). This particular choice is pertinent to the case of oscillatory flows that are the basis of dynamic rheometric testing. As expected, the analysis shows that ability of the instrument to extract surface rheological data improves with increasing Boussinesq number, and this paper offers strategies to extend the useful range of the ISR, as discussed further in Section 6.

In addition to analyzing purely viscous monolayers, Vermant and colleagues (82) consider viscoelastic interfaces that are characterized by both viscous and elastic surface moduli, $G_s'(\omega)$ and $G_s''(\omega)$. In this case, the Boussinesq number can be generalized to the following complex form:

$$Bo(\omega) = \frac{G_s''(\omega) - iG_s'(\omega)}{\omega L \eta}. \quad 12.$$

6. INTERFACIAL RHEOLOGICAL DETERMINATION

Properly designed surface rheometers measure both the stress and deformation history for fluid interfaces at which the constitutive property is not known a priori (83). A rheometer must be able to measure the fundamental material functions, such as the (shear rate–dependent) viscosity and the linear viscoelastic moduli. Gradients in surface tension should be avoided because they will induce unwanted Marangoni flows. Moreover, one should be able to readily analyze the flow field. Similar to their bulk counterparts, surface rheometers can be classified with respect to their kinematics and different types of deformations, i.e., shear (and extensional) rheometry versus dilatational rheometry. In shear rheometry, the interface is deformed while keeping the surface area constant. Both direct and indirect measurement methods have been proposed; the former measure the forces and the deformation, whereas the latter use measurements of the velocity profile to extract the interfacial rheological properties. Not all of the designs presented in the literature have flows that are viscometric, i.e., flows that can be analyzed without prior knowledge of the constitutive properties of the interface. One of the main challenges is that one must deal with the intimate coupling between the interfacial and bulk flows, as discussed in Section 5.

6.1. Shear Measurements at Constant Area

A key design consideration, which was already realized by Lord Rayleigh, is that the contribution from the surface should dominate the force on the measurement probe. Those forces coming from the bulk, owing to the presence of velocity gradients in the surrounding fluid phases, should be minimized. This can be done by minimizing the characteristic length scale of the geometry L in Equation 6 either by decreasing the size of the measurement probe or by realizing that the characteristic length scale is set by the ratio of the contact perimeter between the surface probe and the interface and the contact area with the surrounding subphases. A maximal amount of perimeter for a given contact area (as was used by Lord Rayleigh) gives optimal sensitivity (84, 85).

Figure 5 presents some common types and measurement configurations of interfacial shear rheometers. Myers & Harkins (86) first reported the development of a 2D capillary viscometer, which was based on surface pressure–driven flow in a channel, as shown in **Figure 5*a***. Rotational devices offer more flexibility and include several 2D equivalents of the Couette geometry (87–90) or the double-wall Couette geometry (84). Also, the needle device of Plateau has been revisited, but now the rod is forced to translate (85) such that it is equivalent to the sliding plate rheometer in 3D.

The magnetic rod ISR is the equivalent of the sliding plate rheometer in bulk (85, 91). A magnetic rod is placed at the interface in the center of a channel and set in motion by a magnetic field. An interfacial shear flow is set up between the rod and the walls of the channel. For sufficiently high surface viscosities and relatively small gaps, the velocity profile between the rod and the walls will be linear. As indicated in Section 5, identification of the conditions for which the coupling between the flows in the bulk and at the interface is important can be done in different ways, using

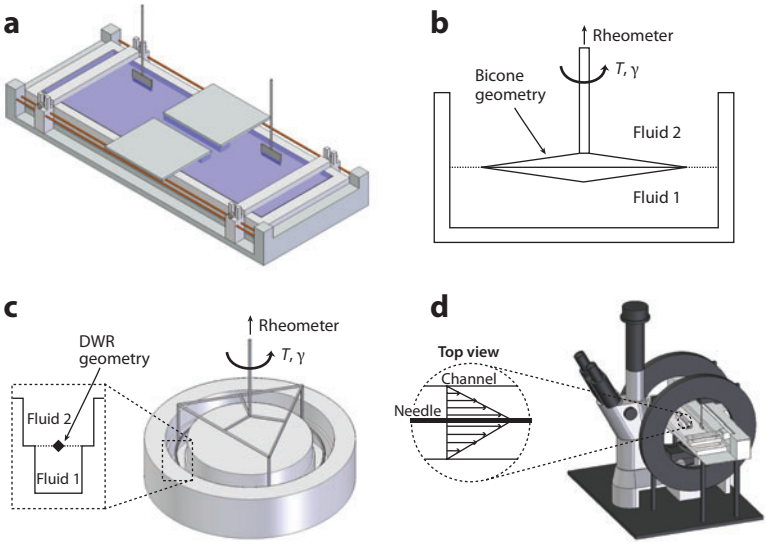

Figure 5

Common types of interfacial shear rheometers: (*a*) surface channel rheometer, (*b*) bicone rheometer (cross section), (*c*) double-wall ring geometry rheometer, and (*d*) interfacial rod rheometer.

analytical solutions (82, 92), numerical methods (91), or experimental verification of the flow profile (82). For large values of *Bo*, a linear profile is obtained, and all material points in the gap essentially move in phase. At $Bo < 100$ the profile deviates from the expected linear one, which has two implications for rheological measurements. First, the value of the shear rate amplitude at the measurement probe will increase as more of the momentum is transferred toward the subphase, close the probe. Because during a surface rheological experiment the interfacial properties are a priori unknown, an iterative procedure is required to obtain the true value of *Bo* and the shear rate to avoid overestimating the magnitudes of the rheological properties. Second, the phase angle between stress and strain, which is important for characterizing viscoelastic fluids, is affected (82).

The 2D equivalent of a double-wall Couette geometry is the double-wall ring (DWR) (84). It maintains the advantage of maximizing the perimeter per unit area but can be mounted onto a sensitive rotational stress rheometer to enable a wide range of rheological tests. Procedures have been developed to calculate the material functions using an iterative process to account for effects of bulk flows. The DWR device offers advantages over the disk and bicone rheometers, which were developed as equivalents of Couette rheometers. Again, setups are available that couple the disk or bicone to a standard rheometer. However, these geometries will always have a larger relative *Bo* than the DWR.

The motion of small probes at the interface also can be used to determine the surface rheological response (93). The use of these microrheological methods, in which the motion of one or two small colloidal probes is monitored to measure the local fluid response, has become increasingly popular (94, 95). The advantages cited are that these measurements should be sensitive and extend to higher frequencies as well as that the transient rheology can be easily monitored, even for small sample volumes, and local-scale heterogeneities can be probed. However, the disturbance flow fields are not rheometric flows, and the analysis relies on the generalized Stokes-Einstein equation or theories that relate the surface diffusion to the surface viscosity (96–99). Strikingly, the experimentally obtained values for the microviscosity are orders of magnitude smaller than those

obtained from macroscopic interfacial rheometers (100). Further theoretical work may be required that takes into account the compressibility of the monolayers or the effects of local Marangoni flows. Recently, Squires and coworkers (64) introduced a novel technique that combines active microrheology with fluorescence microscopy to visualize fluid interfaces as they deform under applied stress, which allows correlation of structure and rheology on the micrometer scale in monolayer films.

6.2. Dilatational Measurements

When the area of a complex interface is increased or decreased, the resulting deformation will result in surface stresses. Contrary to bulk fluids, interfaces are compressible, and one can calculate the Gibbs elasticity (3),

$$E = \frac{\mathrm{d}\sigma}{\mathrm{d}\ln A}, \qquad 13.$$

where E is a measure of the resistance to the creation of gradients in surface tension (or more generally in surface stress). For insoluble monolayers, in the limit of slow deformations, the modulus can hence be obtained from the equilibrium surface pressure isotherm. When the interface is deformed rapidly, either a true rheological response may be present, as a result of the deformed microstructure and friction with the subphases, or responses may be present that are the consequence of other types of transport phenomena. For example, in the case of soluble surfactant monolayers, the diffusion to/from the bulk determines an additional (slow) relaxation process modeled by van den Tempel & Lucassen-Reynders (4). However, recent experiments have shown that the details of the local curvature of drops have an effect on the transport phenomena (101) and hence on the measured relaxation times. For these reasons, it may not be appropriate to identify the measured apparent properties as true material functions.

The experimental techniques that have been designed to measure the dilatational interfacial rheometry are usually based on techniques used for transient interfacial tension, $\sigma(t)$, and the following definition of the transient dilatational modulus,

$$E(t) = \frac{\mathrm{d}\sigma(t)}{\Delta A/A_0}, \qquad 14.$$

is often used for a step strain experiment, and similar definitions can be applied to oscillatory experiments (102). One popular experiment is the oscillating pendant drop or bubble. Often these experiments are analyzed in terms of the Young-Laplace equation, which is certainly not a valid approach for all types of complex fluid interfaces, as discussed in Section 3. In the experiments, either the changes in drop shape are measured as a function of time, which is termed drop shape tensiometry (DST) (103, 104), or the capillary pressure inside the droplet is measured, which is called capillary pressure tensiometry (CPT) (105–107). DST is typically limited to frequencies less than 1 Hz (104). The advantage of CPT is that small spherical droplets can be used, whereas DST employs large drops deformed by gravity. However, a detailed fluid mechanical analysis of these devices is still lacking.

Dilatational experiments on a planar interface also can be performed using a Langmuir-Pockels trough to study longitudinal compressional waves (108–110). This approach is limited to relatively low frequencies. The deformation of the interface is a superposition of shear and dilatational kinematics so that the deformation profile depends on the relative magnitudes of shear and dilatational moduli. For example, highly elastic hydrophobin interfaces display nonuniform deformations (111). To circumvent the problems of inhomogeneous deformations, different approaches, for example using circular barriers or vertically moving ring devices, have been proposed. But even

in these cases, the penetration of the compressional wave in the interface should be taken into account, and the possible coupling of the deformation with flow in the surrounding phases is again of concern. Detailed procedures to calculate the dilatational properties, or at least to identify conditions under which reliable measurements can be performed, are an area of future development. Under some conditions, the shear and dilatational components can be separated by using two Wilhelmy plates, for example as is done in Petkov et al.'s (109) analysis of an elastic interface and more generally for viscoelastic interfaces by Cicuta & Terentjev (110).

Transverse wave damping techniques have also received a fair share of attention. However, the theoretical analysis of wave damping has proven difficult, and effects of surface tension, compressibility, Marangoni flows, and true dilatational rheological material functions all contribute. The capillary wave method became increasingly popular with the advent of laser scattering methods, in particular of surface quasi-elastic light scattering [see, e.g., the recent review by Noskov (112)]. The dispersion relation and the power spectrum are connected to the damping and to the surface rheological properties. Going beyond simple interfaces, Levich (113) was the first to present a rigorous analysis for surfactant-laden interfaces, including the effect of Marangoni flows. However, unphysical results (e.g., negative dilatational viscosities) can still be found in published literature. Recently Buzza and colleagues (114, 115) presented a more general theory for capillary waves and surface quasi-elastic light scattering for an isotropic liquid interface with adsorbed surfactant. They used Scriven's constitutive model for capillary waves and developed and generalized Levich's results to include various interfacial relaxation processes, including diffusive interchange of surfactants and surfactant chain reorientation and relaxation (114, 115). The effects of surface tension still often dominate the measured response, which makes it difficult to reliably extract surface rheological properties in dilatation using these wave damping techniques.

An important interfacial deformation mode that has seen little activity is constrained surface area, extensional flow. Unlike dilatation, which imparts stretching/compression through an associated change in area, this deformation preserves area while stretching fluid elements within the surface in the absence of a significant rotational component. Dimitrijev-Dwyerab & Middelberg (116) have reported on the Cambridge Interfacial Tensiometer, which they claim offers this capability by separating two rods floating within the interface at a prescribed velocity such that the surface elements initially between the rods are stretched in length.

7. APPLICATIONS

The interfacial rheological and microstructural methods discussed above have been applied to numerous classes of complex fluid-fluid interfaces. This section summarizes recent results, and we have organized the wide range of materials into four broad categories. Owing to space constraints, the discussion focuses on interfacial simple shear results. This flow type admits rigorous analysis, and the corresponding interfacial rheometers have been modeled extensively. Similar detailed descriptions of dilatational rheometers involving highly viscoelastic interfaces are not available. However, Miller & Liggieri (117) provide a comprehensive account of results in dilatational interfacial rheometry.

7.1. Fatty Acids, Fatty Alcohols, and Phospholipids

Fatty acids, fatty alcohols, and phospholipids belong to an important class of amphiphiles with the ability to self-assemble to form long-range interfacial structures. Fatty acids and alcohols find wide use as additives to stabilize emulsions and foams, and they can be found in personal products and

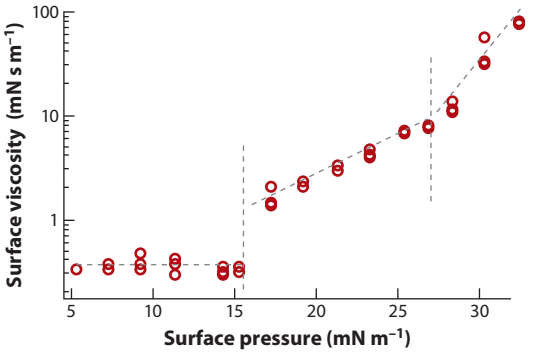

Figure 6

Surface shear viscosity of docosanoic acid as a function of surface pressure. Data from Reference 47.

foodstuffs. Phospholipids are a primary building block in biological membranes, and the structure and dynamics of the monolayers and bilayers they produce have garnered a great deal of attention.

Docosanoic acid (DA) contains 21 carbons in an aliphatic tail attached to a carboxylic acid head group. The room-temperature isotherm of this molecule is shown in **Figure 1**, which indicates several tilt transitions. The tilt of the tails and their intrinsic anisotropy in polarizability leads to layers characterized by anisotropic refractive indices that allow BAM to be used as a convenient method of imaging their polydomain morphology. This was used by Fuller and coworkers (57, 58, 118) to examine the response of DA monolayers to purely extensional, 2D flow using a four-roll mill and to simple shear flow with a parallel band apparatus. This technique reveals that in each phase, the layers display a polydomain structure; each domain has the molecules in the appropriate local arrangement but with different tilt azimuths of the alkyl chain tilt direction.

The phase transitions of DA are accompanied by strong changes in the surface viscosity of these monolayers, as shown in **Figure 6**. The transition from the L_2 phase to the L_2' is signaled by a discontinuous increase in the surface viscosity and a remarkable change in the local molecular dynamics as the alkyl chains of DA respond to hydrodynamic stresses. As reported in Reference 57, in the low-pressure phase, the domains deform affinely with the flow but do not change contrast, which suggests that the tilted alkyl tails do not change their orientation relative to the flow direction. Furthermore, the flow-induced deformation of the domains was reversible. However, in the higher-pressure, L_2' phase, the tilt azimuth rotated by 90° following reversal of the flow direction in the four-roll mill. Unlike the L_2 phase, the L_2' phase did not deform affinely and did not display reversibility in domain shape following flow reversals. Overall, the lower-pressure L_2 phase exhibited the attributes of a Newtonian monolayer, whereas the L_2' phase responded in ways reminiscent of a liquid crystal.

Maruyama et al. (58) also considered DA subjected to simple shear flow generated using a parallel band device. This flow type, which imparts a torque on the monolayer through its vorticity component, also produces important differences in the response of the L_2 and L_2' phases. In **Figure 7*a–c*** successive BAM images are shown as a velocity gradient of 2 s^{-1} is applied to the L_2 phase. The vorticity rotates clockwise in this figure, and as the flow proceeds the intensity contrast of the different domains in the monolayer modulates with time. This is a consequence of the rotation of the tilt azimuth with the vorticity. However, the domains retain their identity, and although their light contrast in the BAM images modulates, the contrast within each domain is spatially uniform. Ignés-Mullol & Schwartz (119) were able to quantify the period of rotation of domain structure as a function of the applied shear rate. The flow response to shear of the L_2'

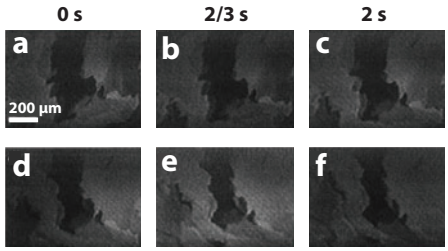

Figure 7

(*a–c*) Brewster angle microscopy (BAM) images of deformation of the domain structure of the L_2 phase of docosanoic acid subject to a simple shear flow of 2 s^{-1}. The velocity gradient is vertical so that the vorticity has a clockwise sense (panel *a*, 0 s; panel *b*, 2/3 s; panel *c*, 2 s). (*d–f*) BAM images of the response of the L_2' phase to a simple shear flow of 2 s^{-1} (panel *d*, 0 s; panel *e*, 2/3 s; panel *f*, 2 s). Shear band propagation occurs within the domain located at the center of the frames. Figure adapted from Maruyama et al. (58).

phase is distinctly different because the molecules in this phase can reorient within each domain, as shown in **Figure 7*d–f***. As the series of BAM images of the domain structure in this figure indicate, shear bands appear within domains as the flow is applied.

Unlike analogous fatty acids, fatty alcohols appear to lack an NN-tilted (L_2) phase. Fewer viscoelastic measurements can be found for these materials. Measurements of the surface shear viscosity and moduli of eicosanol ($C_{20}H_{41}OH$) have been reported using an ISR (45, 85). A maximum was found in the surface viscosity as a function of surface pressure in the L_2' phase. However, the origin of this maximum has not been fully explained.

The viscoelastic properties of phospholipids have been extensively studied. Interfacial rheology plays a central role in two important problems in human health: the dynamics of the lung surfactant coating the alveoli and the meibomian lipid layer coating the tear film. Zasadzinski and coworkers (25, 120) have examined the structure and dynamics of the remarkable mixture of lipids and protein that constitute our lung surfactant. This composition stabilizes the thin aqueous layer coating the alveoli by strongly decreasing its surface tension. Furthermore, the lung surfactant is viscoelastic, and this enhanced elasticity stabilizes the layer against dewetting (121).

The meibomian lipid layer covering the tear film of our eyes is also a mixture of long-chain phospholipids. Exuded by glands in our eyelids upon each blink, this layer is also strongly viscoelastic and has a strong melting transition near physiological temperatures (26). The strong viscoelasticity of this insoluble layer has important implications for the problem of wetting and dewetting of the tear film, and measurements of the advancing contact angle of drops covered with this material revealed a striking "stick-slip" phenomenon that causes these drops to violate the Voinov model of the moving contact line (122). Measurement of the advancing/receding contact angle is a convenient method of appreciating the influence of complex interfacial dynamics on this interfacial flow problem (123).

7.2. Proteins at Interfaces

The interfacial rheology of proteins adsorbed to fluid/fluid interfaces has important consequences for the stability of foams and emulsions. One route to stability in these two-phase materials is the formation of coalescence-arresting viscoelastic skins on the surfaces of drops and bubbles. In contrast to simple amphipathic molecules, most proteins undergo conformation changes (denaturation) upon adsorption because such a step can expose a greater portion of the protein's hydrophobic sequences to air or oil and lower the molecule's free energy. Once denatured,

neighboring proteins can interact, often through disulfide bonds, to generate an interfacial gel that irreversibly resides at the surface. A detailed account of protein-fluid interface interactions can be found in Möbius & Miller (124).

Radke and coworkers (125) investigated both the shear and the dilatational interfacial rheology of two proteins: the globular lysozyme and the disordered β-casein. Lysozyme, which denatures, forms viscoelastic films at the hexadecane/water interface over the course of hours. These films are irreversibly attached, and the elastic interfacial modulus exceeds the viscous modulus. This is not the case for β-casein, which forms interfaces that are predominately viscous with weak elastic responses. The generation of proteinaceous elastic layers on emulsion droplets causes them to resist flow deformation and induces them to precess in shear flow instead of tank treading because the interface can support in-plane shearing stresses. Windhab and coworkers (126) observed these phenomena directly in oil droplets covered with lysozyme layers in simple shear flow.

The interaction between proteins and lipids is fundamental to understanding biological systems such as the lung surfactants and tear films discussed above. These are complex mixtures that involve lipid layers in the midst of protein in solution, and often strong couplings can ensue. For example, Nishimura et al. (127) studied the interaction of lysozyme with a model tear film consisting of a binary mixture of cholesteryl myristate (CM) and DPPC; this protein readily adsorbs onto predeposited lipid monolayers and substantially affects the interfacial rheology.

Another protein prevalent in the body is collagen, a rod-like triple helix that is 300 nm in length. This building block of connective tissue and load-bearing parts is insoluble in water but will form a stable multilayer film (69) at the air/water interface. This is accomplished by spreading collagen dissolved in acetic acid onto the surface. The acid diffuses into the water, leaving the collagen layer behind. Compression of the layer by the barriers of a Langmuir trough orients the collagen fibrils, and this alignment is detectable using dichroism by adding a dye, such as sirius red F3B, into the layer. If the fibril concentration is sufficiently large, the orientation imparted upon compression can persist long enough to accommodate Langmuir-Blodgett deposition of the anisotropic collagen onto solid substrates. Aligned collagen fibrils can provide contact guidance to living cells.

7.3. Particles at Interfaces

As discussed in Section 3, particles can be trapped at interfaces by their capillary energy. However, the presence of an interface adds significant complexity to the colloidal interactions. For example, compared with similar particles in a bulk liquid, the electrostatic repulsion between charged particles is greatly enhanced at a water–low dielectric medium interface, as Pieranski (128) recognized early on. At the interface a particle has an asymmetric counterion distribution that results in a dipole-dipole interaction through the low–dielectric constant phase. The corresponding interaction is repulsive and long range (129). The interaction energy decays inversely with the cube of the separation between the dipoles and is inversely proportional to the electrolyte concentration (130, 131). On one hand, Aveyard et al. (129) suggested that a small number of unscreened surface electric charges, possibly arising from dissociated surface groups and stabilized by water trapped on rough particle surfaces, are responsible for the strong interaction. On the other hand, Masschaele et al. (132) argue that the finite ion sizes of the hydrated ions on the water side need to be taken into account to arrive at quantitative predictions of the electrostatic forces. Another example of increased complexity is that the presence of a particle can distort the interface, which can give rise to (predominantly attractive) lateral capillary interactions, which are particularly important for particles with a nonspherical shape owing to an undulation of the contact line (133, 134).

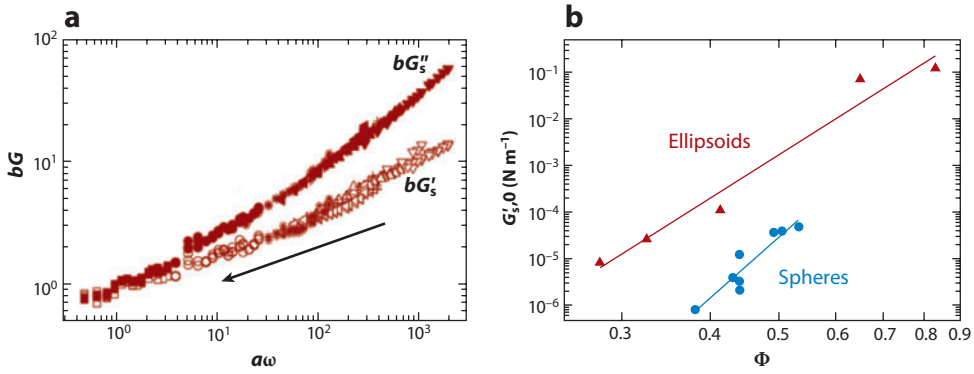

Figure 8

(*a*) Master curve of the scaled values of bG'_S and bG''_S against the scaled frequency ($a\omega$) for a monolayer of colloidal particles; the arrow indicates the direction of increasing surface concentration [from Cicuta et al. (14), *Phys. Rev. Lett.* 90:236101; copyright 2003 © 2003 by the American Physical Society] (*b*) Surface coverage dependency of the storage modulus for aggregated spheres (data from Reference 13) and for ellipsoids with the same properties (data from Reference 134).

For stable suspensions, mostly linear viscoelastic properties have been reported. Owing to enhanced electrostatic interactions, the rheology of colloidal crystals has been studied using model polystyrene lattices. Because of the current sensitivity limits of interfacial rheometers, data have been obtained only at area fractions greater than 0.4 at which, owing to the soft and long-range behavior of the potential, the structure is crystalline and the response is elastic. Similar to 3D systems, the Krieger-Dougherty equation with the correct maximum packing fraction correctly describes the divergence of the elastic moduli near close packing (14). Another similarity is that when the monolayer is compressed, a scaling for the viscoelastic moduli with concentration can be retrieved with a characteristic scaling for soft glassy systems (13). **Figure 8** shows how the linear viscoelastic moduli, taken at different surface coverages and rescaled by a factor b, can be superimposed onto a master curve by rescaling the frequency, ω.

For aggregated suspensions, for which rheological modeling is not yet as advanced, 2D suspensions offer the advantages that the microstructure and its hierarchy can be visualized at high resolution and that the surface coverage can be varied efficiently. The sol-gel transition in 2D systems can be monitored accurately using rheological measurements (14, 135). The linear viscoelastic properties of aggregated 2D suspensions show a power law dependency on concentration similar to that of their 3D counterparts. The values of the power law exponents relating the moduli to the surface coverage are much higher owing to the reduction in dimensionality from 3D to 2D (14). This implies that surface flocculation is an effective way to create interfaces with solid-like rheological properties at a fairly low surface coverage; similar features are observed for the dilatational properties.

Strong surface gels can be made using nonspherical particles to exploit the specific nature of the lateral capillary forces at the interface. A monolayer of ellipsoids exhibits a substantial surface modulus even at low surface coverage and can be used to create even more elastic monolayers than are formed by aggregate networks of spheres of the same size and surface properties (134). This also plays a role in preventing the coffee ring effect (16). Most experiments thus far have focused on linear viscoelastic properties. Transient measurements can be difficult to interpret, as changes in the surface rheology lead to time-dependent flows in the bulk that become more challenging to analyze. Nonlinear rheology in shear (and dilation) remains largely unexplored.

7.4. Polymers at Interfaces

Many polymers are amphiphilic and capable of producing stable Langmuir films. Depending on the structure of the chain, they either can lie flat on the surface, if amphiphilic moieties are distributed along the backbone, or can straddle it, as in the case of block copolymers. The potential for chain entanglements is distinctly different for these two cases. Block copolymers, in which different blocks lie entirely on different sides of an interface, can readily entangle if the chain lengths are sufficiently long. For example, Luap & Goedel (136) found that in linear polyisoprene chains terminated by sulfonated (SO^{-}_{3}) headgroups, the polyisoprene chains extend upward into the air to create a brush consisting of a room-temperature melt. Indeed, the interfacial shear moduli of these systems were remarkably similar to those of bulk, entangled melts and displayed viscous behavior at low frequencies followed by a rubbery plateau in the elastic surface modulus as the frequency was increased.

Entanglements are not possible when the chains lie strictly flat on the surface, as argued by de Gennes (137). Rather than interpenetrate, the chains are predicted to compress as their surface concentration increases. Maier & Rädler (138) followed the dynamics of DNA chains bound electrostatically to cationic supported lipid bilayers. They confirmed that the chains segregate and do not interpenetrate. The dynamics were Rouse-like, and the conformation was fractal.

Poly(*tert*-butyl methacrylate) is a convenient choice for studies of polymer Langmuir films with flat configurations. Gavranovic et al. (44) studied monolayers of this polymer using the ISR and BAM. In the low–surface pressure regime, the surface viscosity was proportional to molecular weight, which agrees with the prediction of noninterpenetrating chains. However, when multilayers formed, surface viscosity became independent of molecular weight; this was attributed to a transition to glassy dynamics because multilayers of this polymer would find themselves below the glass transition temperature.

Monteux et al. (139) studied adsorbed layers of oppositely charged polymer-surfactant complexes at the air-water interface. In this system, the polymer, poly(styrenesulfonate), was decorated with a cationic surfactant, dodecyltrimethylammonium bromide, to form surface-active complexes, with structures and dynamics that depend on the ratio of polymer to surfactant. This is an example of the polymer-surfactant systems that are often used in the stabilization of foams and emulsions, and the work aimed to determine the link between foam stability and the interfacial rheology of these mixtures. Indeed, the results indicated that the stability was optimized at the particular polymer-to-surfactant ratio (in this case equal amounts) that produced a maximum in the elastic interfacial modulus.

Polymer chains that assume the shape of rigid rods have the ability to form liquid crystals. Lyotropic systems, in which the chains are in solution, form these phases at sufficiently high concentration. When constrained to 2D, this order-disorder transition can readily occur and has been observed in several systems. Two polymers have been examined in detail, primarily because they are strongly dichroic in the UV, which allows dichroism to be used to directly measure orientation of the polymer rods. These are poly (phthalocyaninato siloxane), a hairy rod polymer (140, 141), and PPPSH (68). At low surface pressures, monolayers of these rod-like polymers are isotropic. When subjected to surface flows, molecular orientation is revealed through dichroism.

8. CONCLUSIONS

The influence of interfacial rheology is evident in many natural and industrial systems. This has led to increased activity in the development of experimental methods to extract the associated material functions and to explore correlations of interfacial viscoelasticity with observed

phenomena in capillarity, interfacial stability, and interfacial transport. The greatest success in equipment development has occurred in methods for shear rheometry at constant surface area. Conversely, measurements of dilatational and constant area extensional surface rheometry are still problematic and in need of advancement. Microstructural measurements are well developed for some systems, such as particles at interfaces, but molecular-level interrogation of flow-induced orientation is still restricted to highly dichroic materials. The power of GIXD has yet to be applied to flowing systems, although this is possible in principle.

Areas of application continue to be developed, and interfacial rheology is increasingly recognized for its importance in biology. This is a natural consequence of the predominance of complex fluid-fluid interfaces in living systems. The majority of applications, however, have been for monolayer systems such as lung surfactants, meibomian lipids, and the oral cavity. When interfacial rheology has been applied to cellular mechanical responses, lipid monolayers often have been employed as models of leaflets of phospholipid bilayers. Although this approach can yield useful results, it is desirable to develop methods to reveal the viscoelasticity of bilayers and in vivo systems.

DISCLOSURE STATEMENT

The authors are not aware of any affiliations, memberships, funding, or financial holdings that might be perceived as affecting the objectivity of this review.

ACKNOWLEDGMENTS

We would like to thank all our students and collaborators who have contributed to our understanding of these fascinating systems. Tom Verwijlen is specifically acknowledged for his help in preparing some of the figures.

LITERATURE CITED

1. Young T. 1805. An essay on the cohesion of fluids. *Philos. Trans.* 95:65–87
2. Slattery JC, Sagis L, Oh ES. 2006. *Interfacial Transport Phenomena*. New York: Springer. 2nd ed.
3. Gibbs WJ. 1878. On the equilibrium of heterogeneous substances. *Trans. Conn. Acad.* III:108–248, 343–524
4. van den Tempel M, Lucassen-Reynders EH. 1983. Relaxation processes at fluid interfaces. *Adv. Colloid Interface Sci.* 18:281–301
5. Georgieva D, Schmitt V, Leal-Calderon F, Langevin D. 2009. On the possible role of surface elasticity in emulsion stability. *Langmuir* 25:5565–73
6. Maldonado-Valderrama J, Martín-Molina A, Martín-Rodriguez A, Cabrerizo-Vílchez MA, Gálvez-Ruiz MJ, Langevin D. 2007. Surface properties and foam stability of protein/surfactant mixtures: theory and experiment. *J. Phys. Chem.* 111:2715–23
7. Murray BS. 2007. Stabilization of bubbles and foams. *Curr. Opin. Colloid Interface Sci.* 12:232–41
8. Dickinson E. 2003. Hydrocolloids at interfaces and the influence on the properties of dispersed systems. *Food Hydrocolloids* 17:25–39
9. Dorshow RB, Swofford RL. 1989. Application of surface laser-light scattering spectroscopy to the photoabsorbing systems: the measurement of interfacial tension and viscosity in crude oil. *J. Appl. Phys.* 65:3756–59
10. Ramsden W. 1903. Separation of solids in the surface-layers of solutions and "suspensions" (observations on surface-membranes, bubbles, emulsions, and mechanical coagulation). Preliminary account. *Proc. R. Soc. Lond.* 72:156–64
11. Pickering SU. 1907. Emulsions. *J. Chem. Soc.* 91:2001–21

12. Binks BP, Horozov TS. 2005. Aqueous foams stabilized solely by silica nanoparticles. *Angew. Chem. Int. Ed. Engl.* 44:3722–25
13. Cicuta P, Stancik EJ, Fuller GG. 2003. Shearing or compressing a soft glass in 2D: time-concentration superposition. *Phys. Rev. Lett.* 90:236101
14. Reynaert S, Moldenaers P, Vermant J. 2007. Interfacial rheology of stable and weakly aggregated two-dimensional suspensions. *Phys. Chem. Chem. Phys.* 9:6463–75
15. Stancik EJ, Kouhkan M, Fuller GG. 2004. Coalescence of particle-laden fluid interfaces. *Langmuir* 20:90–94
16. Yunker PJ, Still T, Lohr MA, Yodh AG. 2011. Coffee ring effect undone by shape dependent capillary interactions. *Nature* 476:308–11
17. Cates ME, Clegg PS. 2008. Bijels: a new class of soft materials. *Soft Matter* 4:2132–38
18. Mironi-Harpaz I, Narkis M. 2001. Electrical behavior and structure of polypropylene/ultrahigh molecular weight polyethylene/carbon black immiscible blends. *J. Appl. Polym. Sci.* 81:104–15
19. Aussillous P, Quere D. 2001. Liquid marbles. *Nature* 411:924–27
20. McHale G, Newton MI. 2011. Liquid marbles: principles and applications. *Soft Matter* 7:5473–81
21. Xue Y, Wang H, Zhao Y, Dai L, Feng L, et al. 2010. Magnetic liquid marbles: A precise miniature reactor. *Adv. Mater.* 22:4814–18
22. Binks BP, Murakami R. 2006. Phase inversion of particle-stabilized materials from foams to dry water. *Nat. Mater.* 5:865–69
23. McConnell HM. 1991 Structures and transitions in lipid monolayers at the air-water interface. *Rev. Phys. Chem.* 42:171–95
24. Noguchi H, Gompper G. 2005. Shape transitions of fluid vesicles and red blood cells in capillary flows. *Proc. Natl. Acad. Sci. USA* 102:14159–64
25. Zasadzinski JA, Ding J, Warriner HE, Bringezu F, Waring F. 2001. The physics and physiology of lung surfactants. *Curr. Opin. Colloid Interface Sci.* 6:506–13
26. Leiske DL, Raju SR, Ketelson HA, Millar TJ, Fuller GG. 2010. The interfacial viscoelastic properties and structure of human and animal Meibomian lipids. *Exp. Eye Res.* 90:598–604
27. Daniels R, Reynaert S, Hoekstra H, Verreth C, Janssens J, et al. 2006. Quorum signal molecules as biosurfactants affecting swarming in *Rhizobium etli*. *Proc. Natl. Acad. Sci. USA* 103:14965–70
28. Fauvart M, Phillips P, Bachaspatimayum D, Verstraeten N, Fransaer J, et al. 2012. Surface tension gradient control of bacterial swarming in colonies of *Pseudomonas aeruginosa*. *Soft Matter* 8:70–76
29. Angelini TE, Roper M, Kolter R, Weitz D. 2009. *Bacillus subtilis* spreads by surfing on waves of surfactant. *Proc. Natl. Acad. Sci. USA* 106:18109–13
30. Franklin B. 1774. Of the stilling of waves by means of oil. *Philos. Trans.* 64:445–60
31. Tanford C. 2004. *Ben Franklin Stilled the Waves: An Informal History of Pouring Oil on Water with Reflections on the Ups and Downs of Scientific Life in General*. New York: Oxford Univ. Press
32. Rayleigh L. 1889–1890. Measurements of the amount of oil necessary in order to check the motions of camphor upon water. *Proc. R. Soc. Lond.* 47:364–67
33. Pockels A. 1891. Surface tension. *Nature* 43:437
34. Plateau JAF. 1873. *Statique Expérimentale et Théorique des Liquides Soumis aux Seules Forces Moléculaires*. Paris: Gauthier-Villars
35. Marangoni C. 1872. The principle of the surface viscosity of liquids established by Mr. J. Plateau. *Nuovo Cimento 2*, Ser. 2:239–73
36. Rayleigh L. 1890. On the superficial viscosity of water. *Proc. R. Soc. Lond.* 48:127–40
37. Boussinesq J. 1913. Existence of a superficial viscosity in the thin transition layer separating one liquid from another contiguous fluid. *C. R. Acad. Sci.* 156:983–89
38. Lebedev AA. 1916. Stokes' law as applied to liquid balls. *J. Russ. Phys. Chem. Soc. Part. Phys.* 48:97–131
39. Silvey A. 1916. The fall of mercury droplets in a viscous medium. *Phys. Rev.* 7:106–11
40. Scriven LE. 1960. Dynamics of a fluid interface. Equation of motion for Newtonian surface. *Chem. Eng. Sci.* 12:98–108
41. Shuttleworth R. 1950. The surface tension of solids. *Proc. Phys. Soc.* A63:445–57
42. Rayleigh L. 1890. On the theory of surface forces. *Philos. Mag.* 30:285–98, 456–75

43. Freer E, Yim KS, Fuller GG, Radke C. 2004. Interfacial rheology of globular and flexible proteins at the hexadecane/water interface: comparison of shear and dilatation deformation. *J. Chem. Phys.* 108:3835–44
44. Gavranovic G, Deutsch J, Fuller G. 2005. Two-dimensional melts: polymer chains at the air-water interface. *Macromolecules* 38:6672–79
45. Kurtz R, Lange A, Fuller G. 2006. Interfacial rheology and structure of straight-chain and branched fatty alcohol mixtures. *Langmuir* 22:5321–27
46. Ghaskadvi GH, Ketterson JB, MacDonald RC, Dutta P. 1997. Apparatus to measure the shear modulus of Langmuir monolayers as functions of strain amplitude and frequency. *Rev. Sci. Instrum.* 68:1792–96
47. Yim KS, Fuller G. 2003. Influence of phase transition and photoisomerization on interfacial rheology. *Phys. Rev. E* 67:041601
48. Als-Nielsen J, Kjaer K. 1989. X-ray reflectivity and diffraction studies of liquid surfaces and surfactant monolayers. *Proc. NATO Adv. Study Inst. Phase Transit. Soft Condens. Matter*, *Geilo*, *Norway*, April 4–14, pp. 113–38. New York: Plenum
49. Aveyard R, Binks BP, Clint JH. 2003. Emulsions stabilised solely by colloidal particles. *Adv. Colloid Interface Sci.* 100–2:503–46
50. Danov KD, Kralchevsky PA, Boneva MP. 2004. Electrodipping force acting on solid particles at a fluid interface. *Langmuir* 20:6139–51
51. de Gennes P-G, Brochard-Wyart F, Quéré D. 2004. *Capillarity and Wetting Phenomena: Drops*, *Bubbles*, *Pearls*, *Waves*. New York: Springer Sci. Bus. Media
52. Stone HA, McConnell HM. 1995. Hydrodynamics of quantized shape transitions of lipid domains. *Proc. R. Soc. Lond. A* 448:97–111
53. Schwartz D, Knobler C, Bruinsma R. 1994. Direct observation of Langmuir monolayer flow through a channel. *Phys. Rev. Lett.* 73:2841–44
54. Olson D, Fuller GG. 2000. Contraction and expansion flows of Langmuir monolayers. *J. Non-Newton. Fluid Mech.* 89:187–207
55. Stancik E, Hawkinson A, Fuller GG, Vermant J. 2004. Dynamic transitions and oscillatory melting of a two-dimensional crystal subjected to shear flow. *J. Rheol.* 48:159–73
56. Masschaele K, Fransaer J, Vermant J. 2009. Direct visualization of yielding in model two-dimensional colloidal gels subjected to shear flow. *J. Rheol.* 53:1437–60
57. Maruyama T, Fuller GG, Frank CW, Robertson CR. 1996. Flow-induced molecular orientation of a Langmuir film. *Science* 274:233–35
58. Maruyama T, Lauger J, Fuller GG, Frank C, Robertson CR. 1998. Orientation in a fatty acid monolayer: effect of flow type. *Langmuir* 14:1836–45
59. Robinson DJ, Earnshaw JC. 1992. Experimental study of colloidal aggregation in two dimensions. I. Structural aspects. *Phys. Rev. A* 46:2045–54
60. Reynaert S, Moldenaers P, Vermant J. 2006. Control over colloidal aggregation in monolayers of latex particles at the oil-water interface. *Langmuir* 22:4936–45
61. Srinivasa KR, Rajagopalan R. 1998. Interaction forces in quasi-two-dimensional charged dispersions. *Phys. Rev. E* 57:3227–33
62. Tarimala S, Ranabothu S, Vernetti J, Dai L. 2004. Mobility and in situ aggregation of charged microparticles at oil-water interfaces. *Langmuir* 20:5171–73
63. Herzig EM, White KA, Schofield AB, Poon WCK, Clegg PS. 2007. Bicontinuous emulsions stabilized solely by colloidal particles. *Nat. Mater.* 6:966–70
64. Choi SQ, Steltenkamp S, Zasadzinski JA, Squires TM. 2011. Active microrheology and simultaneous visualization of sheared phospholipid monolayers. *Nat. Commun.* 2:312
65. Hénon S, Meunier J. 1991. Microscope at the Brewster angle: direct observation of first-order phase transitions in monolayers. *Rev. Sci. Instrum.* 62:936–39
66. Hönig D, Möbius D. 1991. Direct visualization of monolayers at the air-water interface by Brewster angle microscopy. *J. Phys. Chem.* 95:4590–92
67. Fuller GG. 1995. *Optical Rheometry of Complex Fluids*. New York: Oxford Univ. Press
68. Yim KS, Brooks C, Fuller G, Datko A, Eisenbach C. 2000. Non-Newtonian rheology of liquid crystalline polymer monolayers. *Langmuir* 16:4325–32

69. Goffin A, Rajadas J, Fuller GG. 2010. Interfacial flow processing of collagen. *Langmuir* 26:3514–21
70. Daillant J, Bellet-Amalric E, Braslau A, Charitat T, Fragneto G, et al. 2005. Structure and fluctuations of a single floating lipid bilayer. *Proc. Natl. Acad. Sci. USA* 102:11639–44
71. Kaganer V, Möhwald H, Dutta P. 1991. Structure and phase transitions in Langmuir monolayers. *Rev. Mod. Phys.* 71:779–819
72. Daillant J. 2009. Recent developments and applications of grazing incidence scattering. *Curr. Opin. Colloid Interface Sci.* 14:396–401
73. Thomson J. 1855. On certain curious motions observable at the surfaces of wine and other alcoholic liquors. *Philos. Mag.* 10:330–33
74. Marangoni C. 1865. *On the expansion of a drop of liquid floating in the surface of another liquid.* PhD thesis, Università degli Studi di Padova, Italy
75. Leal LG. 2007. *Advanced Transport Phenomena: Fluid Mechanics and Convective Transport Processes*. New York: Cambridge Univ. Press
76. Entov VM, Hinch EJ. 1997. Effect of a spectrum of relaxation times on the capillary thinning of a filament of elastic liquid. *J. Non-Newton. Fluid Mech.* 72:31–53
77. McKinley GH, Tripathi A. 2000. How to extract the Newtonian viscosity from capillary breakup measurements in a filament rheometer. *J. Rheol.* 44:653–70
78. Tomotika S. 1935. On the instability of a cylindrical thread of a viscous liquid surrounded by another viscous fluid. *Proc. R. Soc. Lond. Ser. A* 150:322–37
79. Fermigier M, Limat L, Wesfreid JE, Boudinet P, Quilliet C. 1992. Two-dimensional patterns in the Rayleigh-Taylor instability of thin films. *J. Fluid Mech.* 236:349–83
80. Stone HA. 1995. Fluid motion of monomolecular films in a channel flow geometry. *Phys. Fluids* 7:2931–37
81. Kurnaz M, Schwartz D. 1997. Channel flow in a Langmuir monolayer: unusual velocity profiles in a liquid-crystalline mesophase. *Phys. Rev. E* 56:3378–84
82. Verwijlen T, Moldenaers P, Stone HA, Vermant J. 2011. Study of the flow field in the magnetic rod interfacial stress rheometer. *Langmuir* 27:9345–58
83. Macosko CW. 1994. *Rheology: Principles, Measurements, and Applications*. New York: Wiley-VCH
84. Vandebril S, Franck A, Fuller GG, Moldenaers P, Vermant J. 2010. A double wall-ring geometry for interfacial shear rheometry. *Rheol. Acta* 49:131–44
85. Brooks CF, Fuller GG, Frank CW, Robertson CR. 1999. An interfacial stress rheometer to study rheological transitions in monolayers at the air-water interface. *Langmuir* 15:2450–59
86. Myers RJ, Harkins WD. 1937. The viscosity (or fluidity) of liquid or plastic monomolecular films. *J. Chem. Phys.* 5:601
87. Brown AG, Thuman WC, McBain JW. 1953. The surface viscosity of detergent solutions as a factor in foam stability. *J. Colloid Sci.* 8:491–507
88. Oh SG, Slattery JC. 1978. Disk and biconical interfacial viscometers. *J. Colloid Sci.* 67:516–25
89. Ghaskadvi RS, Dennin M. 1998. A two-dimensional Couette viscometer for Langmuir monolayers. *Rev. Sci. Instrum.* 69:3568–72
90. Erni P, Fischer P, Windhab EJ, Kusnezov V, Stettin H, Läuger J. 2003. Stress- and strain-controlled measurements of interfacial shear viscosity and viscoelasticity at liquid/liquid and gas/liquid. *Rev. Sci. Instrum.* 74:4916–24
91. Reynaert S, Brooks CF, Moldenaers P, Fuller GG, Vermant J. 2008. Analysis of the magnetic rod interfacial stress rheometer. *J. Rheol.* 52:261–85
92. Fischer TM. 2004. The drag on needles moving in a Langmuir monolayer. *J. Fluid Mech.* 498:123–37
93. Tomlinson C. 1860–1862. On the motions of camphor on the surface of water. *Proc. R. Soc. Lond.* 11:575–77
94. Prasad V, Koehler SA, Weeks ER. 2006. Two-particle microrheology of quasi-2D viscous systems. *Phys. Rev. Lett.* 97:176001
95. Ortega F, Ritacco H, Rubio RG. 2010. Interfacial microrheology: particle tracking and related techniques. *Curr. Opin. Colloid Interface Sci.* 15:237–45
96. Saffman PG, Delbrück M. 1975. Brownian motion in biological membranes. *Proc. Natl. Acad. Sci. USA* 72:3111–13

97. Dimova R, Danov K, Pouligny B, Ivanov IB. 2000. Drag of a solid particle trapped in a thin film or at an interface: influence of surface viscosity and elasticity. *J. Colloid Interface Sci.* 226:35–43
98. Sickert M, Rondelez F. 2003. Shear viscosity of Langmuir monolayers in the low-density limit. *Phys. Rev. Lett.* 90:126104
99. Fischer TM, Dhar P, Heinig P. 2006. The viscous drag of spheres and filaments moving in membranes or monolayers. *J. Fluid Mech.* 558:451–75
100. Maestro A, Bonales LJ, Ritacco H, Rubio RG. 2011. Surface rheology: macro- and microrheology of poly(tert-butyl acrylate) monolayers. *Soft Matter* 7:7761–71
101. Alvarez NJ, Walker LM, Anna SL. 2010. Diffusion-limited adsorption to a spherical geometry: the impact of curvature and competitive time scales. *Phys. Rev. E.* 82:011604
102. Miller R, Loglio G, Tesei U, Schano KH. 1991. Surface relaxations as a tool for studying dynamic interfacial behaviour. *Adv. Colloid Interface Sci.* 37:73–96
103. Benjamins J, Cagna A, Lucassen-Reynders EH. 1995. Viscoelastic properties of triacylglycerol/water interfaces covered by proteins. *Colloids Surf. A* 114:245–54
104. Leser ME, Acquistapace S, Cagna A, Miller R. 2005. Limits of oscillation frequencies in drop and bubble shape tensiometry. *Colloids Surf. A* 261:25–28
105. Mysels KJ. 1986. Improvements in the maximum-bubble-pressure method of measuring surface tension. *Langmuir* 4:428–32
106. Nagarajan R, Koczo K, Erdo E, Wasan DT. 1995. Controlled drop tensiometer for measuring dynamic interfacial and film tension. *AIChE J.* 41:915–23
107. Liggieri L, Attolini V, Ferrari M, Ravera F. 2002. Measurement of the surface dilational viscoelasticity of adsorbed layers with a capillary pressure tensiometer. *J. Colloid Interface Sci.* 255:225–35
108. Lucassen J, Vandente M. 1975. Longitudinal waves on viscoelastic surfaces. *J. Colloid Interface Sci.* 41:491–98
109. Petkov JT, Gurkov TD, Campbell BE, Borwankar RP. 2000. Dilatational and shear elasticity of gel-like protein layers on air/water interface. *Langmuir* 16:3703–11
110. Cicuta P, Terentjev EM. 2005. Viscoelasticity of a protein monolayer from anisotropic surface pressure measurements. *Eur. Phys. J. E* 16:147–58
111. Aumaitre E, Vella D, Cicuta P. 2001. On the measurement of the surface pressure in Langmuir films with finite shear elasticity. *Soft Matter* 7:2530–37
112. Noskov BA. 2009. Interfacial elasticity studied by wave methods. See Ref. 116, pp. 103–36
113. Levich VG. 1962. *Physicochemical Hydrodynamics*. New York: Prentice-Hall
114. Buzza DMA, Jones JL, McLeish TCB. 1998. Theory of surface light scattering from a fluid-fluid interface with adsorbed polymeric surfactants. *J. Chem. Phys.* 109:5008–24
115. Buzza DMA. 2002. General theory for capillary waves and surface light scattering. *Langmuir* 18:8418–35
116. Dimitrijev-Dwyerab M, Middelberg A. 2011. The extensional viscoelasticity of protein-coated interfaces. *Soft Matter* 7:7772–81
117. Miller R, Liggieri L, eds. 2009. *Progress in Colloid and Interface Science*. Vol. 1: *Interfacial Rheology*. Leiden: Brill
118. Friedenberg MC, Fuller GG, Frank CW, Robertson CR. 1996. Direct visualization of flow-induced anisotropy in a fatty acid monolayer. *Langmuir* 12:1594–99
119. Ignés-Mullol J, Schwartz DK. 2001. Shear-induced molecular precession in a hexatic Langmuir monolayer. *Nature* 348:348–51
120. Ding J, Warriner H, Zasadzinski J, Schwartz D. 2002. Magnetic needle viscometer for Langmuir monolayers. *Langmuir* 18:2800–6
121. Anseth J, Goffin A, Fuller G, Ghio A, Kao P, Upadhyay D. 2005. Lung surfactant gelation induced by epithelial cells exposed to air pollution or oxidative stress. *Am. J. Respir. Cell Mol. Biol.* 33:161–68
122. Voinov OV. 1976. Inclination angles of the boundary in moving liquid layers. *Fluid Dyn.* 11:714–21
123. Leiske D, Monteux C, Senchyna M, Ketelson H, Fuller G. 2011. Influence of surface rheology on dynamic wetting of droplets coated with insoluble surfactants. *Soft Matter* 7:7747–53
124. Möbius D, Miller R. 1998. *Proteins at Liquid Interfaces*. Amsterdam: Elsevier

125. Freer E, Yim KS, Fuller GG, Radke C. 2004. Interfacial rheology of globular and flexible proteins at the hexadecane/water interface: comparison of shear and dilatation deformation. *J. Phys. Chem. B* 108:3835–44
126. Erni P, Fischer P, Windhab E. 2004. Deformation of single emulsion drops covered with a viscoelastic adsorbed protein layer in simple shear flow. *Appl. Phys. Lett.* 87:244104
127. Nishimura S, Magana G, Ketelson H, Fuller G. 2008. The effect of lysozyme adsorption on the interfacial rheology of DPPC and cholesteryl myristate. *Langmuir* 24:11728
128. Pieranski P. 1980. Two-dimensional interfacial colloidal crystals. *Phys. Rev. Lett.* 45:569–72
129. Aveyard R, Clint JH, Nees D, Paunov VN. 2000. Compression and structure of monolayers of charged latex particles at air/water and octane/water interfaces. *Langmuir* 16:1969–79
130. Hurd AJ. 1985. The electrostatic interaction between interfacial colloidal particles. *J. Phys. A* 18:1055–60
131. Moncho-Jordá A, Martínez-López F, González AE, Hidalgo-Álvarez R. 2002. Role of long-range repulsive interactions in two-dimensional colloidal aggregation: experiments and simulations. *Langmuir* 18:9183–91
132. Masschaele K, Park BJ, Furst EM, Fransaer J, Vermant J. 2011. Finite ion-size effects dominate the interaction between charged colloidal particles at an oil-water interface. *Phys. Rev. Lett.* 105:048303
133. Loudet JC, Alsayed AM, Zhang J, Yodh AG. 2005. Capillary interactions between anisotropic colloidal particles. *Phys. Rev. Lett.* 94:018301
134. Basavaraj MG, Fuller GG, Fransaer J, Vermant J. 2009. Self-assembly and rheology of ellipsoidal particles at interfaces. *Langmuir* 25:2718–28
135. Tadjoa O, Cassagneau P, Chapel JP. 2009. Two-dimensional sol-gel transition in silica alkoxides at the air-water interface. *Langmuir* 25:1205–9
136. Luap C, Goedel W. 2001. Linear viscoelastic behavior of end-tethered polymer monolayers at the air/water interface. *Macromolecules* 34:1343–51
137. de Gennes P-G. 1979. *Scaling Concepts in Polymer Physics*. Ithaca, NY: Cornell Univ. Press
138. Maier B, Rädler J. 1999. Conformation and self-diffusion of single DNA molecules confined to two dimensions. *Phys. Rev. Lett.* 82:1911–14
139. Monteux C, Fuller G, Bergeron V. 2004. Shear and dilational surface rheology of oppositely charged polyelectrolyte/surfactant microgels adsorbed at the air-water interface. Influence on foam stability. *J. Phys. Chem. B* 108:16473–82
140. Maffettone PL, Grosso M, Friedenberg M, Fuller GG. 1996. Extensional flow of a two-dimensional polymer liquid crystal. *Macromolecules* 29:8473–78
141. Maruyama T, Fuller G, Grosso M, Maffettone PL. 1998. The dynamics of two dimensional polymer nematics. *J. Non-Newton. Fluid Mech.* 76:233–47

Annual Review of Chemical and Biomolecular Engineering

Volume 3, 2012

Contents

Indexes

Errata

An online log of corrections to *Annual Review of Chemical and Biomolecular Engineering* articles may be found at http://chembioeng.annualreviews.org/errata.shtml